UNIVERSITY OF CALIFORNIA SAN DIEGO

Mechanistic Understanding of Mechanoluminescence in ZnS:Cu-PDMS Composite

A Thesis submitted in partial satisfaction of the requirements
for the degree Master of Science

in

Engineering Sciences (Mechanical Engineering)

by

Joshua Aaron Yun

Committee in charge:

Professor Shengqiang Cai, Chair
Professor Javier Garay
Professor Nicholas Gravish

2023

The Thesis of Joshua Aaron Yun is approved, and it is acceptable in quality and form for publication on microfilm and electronically.

University of California San Diego

2023

DEDICATION

To my friends and family, without your encouragement, support, and reminders to occasionally smell the roses this work would not have been possible.

EPIGRAPH

Who do you think you are! One contributes what one can!

-Attributed to Stephen Timoshenko by YC Fung

TABLE OF CONTENTS

LIST OF FIGURES

LIST OF ABBREVIATIONS

PDMS	Polydimethylsiloxane
ML	Mechanoluminescence
EML	Elastico-mechanoluminescence

LIST OF SUPPLEMENTAL VIDEOS

Yun_Compression100cycles_5hz_S50.avi

Yun_Constrainedseparation_5hz_S50.avi

Yun_Sliding_05hz_10mm.avi

ACKNOWLEDGEMENTS

I would like to thank Professor Shengqiang Cai and the other members of the Cai Lab for their continued curiosity and enthusiasm for inquiry, it has been an inspiring example.

Chapters 2,3,4,5,6,7, and 8 contain material which is being prepared for publication. Yun, Joshua; Li, Chenghai; Cai, Shengqiang. The thesis author was the primary researcher and co-author of this publication.

ABSTRACT OF THE THESIS

Mechanistic Understanding of Mechanoluminescence in ZnS:Cu-PDMS Composite

by

Joshua Aaron Yun

Master of Science in Engineering Sciences (Mechanical Engineering)

University of California San Diego, 2023

Professor Shengqiang Cai, Chair

For ZnS:Cu-PDMS composites, the high durability and repeatable light emission due to mechanical stimuli shows promise in various sensing and signaling applications as a method of adding functionality without a dedicated external power source. The cause-and-effect relationship between mechanical loading and light emission in the composite has been widely studied, but there are remaining gaps in understanding of the nature of the mechanical interaction between the particles and matrix and how this affects light emission. Simplified experiments of compressive and sliding interaction and visual observations of the particle-matrix interface provide insight into the nature of

the physical interactions that lead to luminescence. Light response to variation of tensile loading characteristics, strain and strain rate, as well as well as the sample characteristics of particle size and mix ratios are compared. Finally, a close examination of the evolution of the light and stress response to cyclic tensile loading shows support for the role that stress softening and interfacial separation play in the characteristics of the light response. The improved understanding can help guide efforts to optimize the material for different applications.

CHAPTER 1: BACKGROUND

1.1 Luminescence and Materials

Luminescence refers to the non-thermal emission of light due to excitation of a material by an external source (1). Depending on the material, triggers for luminescence can include an external electric field, UV light, chemical, or mechanical stimuli (1,2,3). The stimuli induce processes that excite electrons in the materials from the valence band to the conduction band which then emit photons that are observed in the visible spectrum as light when returning to their lower energy states. This work will focus on the emission of light due to mechanical stimuli, generally referred to as mechanoluminescence (ML).

Types of ML are generally broken into subcategories based on stimuli. These categories can include: fractoluminescence, triboluminescence, and elastico-mechanoluminescence (EML) which are dependent on material fracture, frictional interaction, and elastic deformation respectively (2). Triboluminescence and EML have the advantage that they are repeatable processes, while fractoluminescence operates destructively.

ML has been observed in both biological systems and inorganic compounds (4,5). The color of the emission and the intensity and duration of the light can change dependent on the phosphor (1,2). The phosphor of interest in this work, ZnS:Cu particles, have been shown to have useful properties of repeatability of emission when combined within a polydimethylsiloxane (PDMS) matrix (6). PDMS is useful as a matrix material due to its thermal and mechanical stability as well as its relative chemically inert behavior when cured. The composite material can be stretched to high strains, resulting in light emission, repeatedly without failure. With Cu acting as a dopant material in the ZnS crystal structure, the light emitted appears as blue-green in color (6). Light emitted from the material is relatively stable from cycle to cycle and can be of high enough intensity to be observed by eye in a dark room.

1.2 Applications From Literature

Due to the repeatable nature of the light emission and sensitivity to mechanical stimuli, ZnS:Cu-PDMS composite material shows promise in multiple applications. Although it can be triggered by

dedicated electric fields, the light emission does not require a dedicated electrical power source to trigger and as a result it has been proposed that it would be useful in sensors for structural health monitoring, wearable devices, displays, soft robotics, and other applications where a dedicated power source may be impractical (1,2,3,7).

The characteristic of light emission of the material to mechanical loading naturally lends the composite as a candidate for sensing and visualizing strain over an area. It can be adhered to a surface and as the surface experiences strain, will also cause strain and light emission in the composite (8-10). This may act as either an indicator of strain in the underlying material or as a tactile sensor as the composite comes into contact with an object.

The material has also been demonstrated for use as a visual marker for tracking small robots, it can be combined with elastomeric actuators and take advantage of the same electric field that powers the actuation to luminesce (11). This luminescence can then be used to track movement.

It can similarly be activated by sound waves in a fluid as well as directly applied strain and used to visualize sound. As a membrane, it was shown that the material could mimic the basilar membrane within the cochlea in the human ear and demonstrate selective light responses to different frequencies (12).

In remote regions it could also serve as a source of light allowing for sustainable lighting. Under proper conditions the composite can luminesce under a wind loading, converting the mechanical wind energy into light (13).

There may also be opportunities for the material as a way of mitigating potentially destructive surface charge buildup. It has recently been shown that a similar composite has the property of converting surface charges into light when strained (14).

It has also been shown to be capable of use in a fiber or fabric type application, enabling the use of woven meshes to create a kind of mechanically driven display (15).

The promise of added capability without additional dedicated external power sources provides a wealth of opportunities of applications.

1.3 Previous Experimental Work

In order to optimize the material for different applications, many prior studies in literature have been conducted to understand functional characteristics of light emission from the composite. These characteristics are related to the composition, characteristics of stimuli, as well as the geometry of the composite.

Generally, an increase in weight percent of the phosphor in the sample relative to the PDMS matrix will increase the light emission. Proportions of up to 70% have been shown to exhibit this behavior while maintaining elasticity of the sample (15,16). An increase in sample thickness within a certain regime can also be shown to increase light intensity (15,16).

A locally applied force, such as writing on the surface with a pen, has also been shown to enhance the luminescence. After applying the force, ultrasonication in the dark caused the writing pattern to reappear as a luminescent glow (16).

Increasing the frequency of cyclic loading or increasing the strain has also been shown to increase the intensity of light emission (15,17).

A sample with engineered cracks has been found to increase the maximum light intensity emitted in the region of the crack defect (18,19). The presence of the macroscopic defect tends to increase the stress concentration locally, resulting a higher sensitivity to low strains.

The relationship of the light to applied strain has been shown to have a non-monotonic behavior. During a single tensile loading cycle of stretching and relaxation, light has been recorded as having two instances of major emission (6,20,21). These peaks of emission do not generally occur at the time of maximum or minimum strain of a cycle.

Frequently, studies are performed on samples subjected to multiple cycles (6,9,15). When cycled multiple times it can be observed that the pattern of light response of the material is largely repeatable after a number of cycles.

1.4 Previous Understanding of ML Mechanism

Many prior works have focused on the relative effects of varying the mechanical stimulus, the material geometry, or processing on light emission (8,15-19). Often, these studies also include an explanation of the mechanism behind the emission as context. For the emission of ZnS:Cu-PDMS composite there are two primary theories. The first theory is based on the coupled effect of piezoelectrically induced charge or dislocation movement coupled with a photoelectric effect, the second relies on triboelectric charge from the frictional interaction of the particle and matrix.

The first explanation is the piezoelectrically driven excitation and emission. It relates the deformation induced in the ZnS:Cu particles from the matrix during mechanical loading to the emission of light (22,23). A more recent theory has emerged from Sohn that the light is the result of frictional interactions that lead to triboelectric charge at the particle and matrix interfaces (21). There are multiple characteristics of both the materials and the light emission that provide clues to the most likely explanation and better understand the mechanism of emission.

1.5 Overview

In order to realize optimal uses of the material characteristics, a more detailed framework for understanding the driving mechanisms of light emission is useful in guiding investigations of potential applications. To better understand the nature of the mechanical interaction between the particles and matrix in the composite that causes light emission, several different experiments were conducted.

Custom setups were assembled to investigate simplified interactions between the particles and matrix material. By attempting to minimize the effects of frictional interactions, relative contributions of the frictional interaction and applied loading to light emission are examined.

Tensile samples of the composite were used to observe the effects of varying the external stimuli as well as the characteristics of the constituent materials. Variation of the applied strain and strain rates were used to investigate their effect on the light emission response. Effects of the characteristics of the two constituents were investigated by varying particle size of the ZnS:Cu and mix ratios of the PDMS.

Geometry of the tensile samples were modified to observe stress concentration effects. Holes were created in samples to induce stress concentrations and light emission response is measured along an axis to observed the effect.

The effects of loading history on the composite were also investigated to provide insight into the driving cause of the change in light emission response. By observing the evolution of the light and stress response to multiple cycles of loading from initial to steady, repeated behavior of the mechanism can be clarified.

To investigate the emission decay behavior and the intensity of emission at different strain levels, strain is increased in small increments on a tensile sample and allowed to decay before increasing strain again. Maximum intensity from different increments is compared to observe overall behavior and explained by a distribution of strain levels required to cause emission at different particle interfaces. Light emission from different strain levels is fitted and decay characteristic estimated.

CHAPTER 2: FABRICATION AND TESTING METHODS

2.1 Preparation of Tensile Samples

Each prepared sample was a composite material containing particles of ZnS:Cu encapsulated in a matrix of PDMS. The PDMS used was commercially available Wacker ELASTOSIL® RT 601 A/B. This PDMS is a two-part, platinum catalyzed, room temperature vulcanization silicone that was selected due to the high optical clarity. Except in the case of experiments performed to observed the effects of different mix ratios, the PDMS was prepared with the manufacturer recommended ratio of 9:1 part A to part B (24). It has a reported value of Shore A hardness of 45 and a tensile strength of 6 MPa (24). The ZnS:Cu particles were used as supplied by Tianjin ZhongYuanXing TT Co, LTD without further purification or treatment unless otherwise noted.

To prepare samples, a Thinky mixer was used at 2000 RPM for 30 seconds to create a homogenous mixture of 50% weight ZnS:Cu and 50% weight PDMS. The mixture was then cast with a nominal thickness of 0.5mm into an open-faced mold and allowed to cure at room temperature for 12 hours. After the composite had set, it was cut into individual rectangular pieces 8mm wide and 40 mm long from the cast sheet and adhered to 3mm thickness acrylic blocks using a commercial silicone sealant, Loctite® Clear Silicone Sealant 2.7 oz 1700009 en-US. Prior to bonding the sample to the acrylic blocks, 3M aluminum oxide sandpaper was used to prepare the bonding surface of the acrylic by removing surface gloss and increasing surface roughness. Any remaining sanding residue was removed before applying the sealant to the surface and assembly of the sample. The prepared sample was then placed in an oven for at least 24 hours at 85° C. When removed from the oven, the sample was allowed to cool to room temperature before testing. The resultant tensile sample was 8mm wide by 16mm tall and 0.5mm thick. Unless otherwise noted, tensile samples were manufactured and assembled to these dimensions.

2.2 Preparation of Optical Microscopy Samples

The prepared sample used in the optical microscope observations was a composite material containing particles of ZnS:Cu encapsulated in a matrix of PDMS with an additional layer of PDMS cast on top. The PDMS used was commercially available ELASTOSIL® RT 601 A/B. The PDMS was prepared with the manufacturer recommended ratio of 9:1 part A to part B. The ZnS:Cu particles were used as supplied by Tianjin ZhongYuanXing TT Co, LTD without further purification or treatment unless otherwise noted.

To prepare the sample, a Thinky ARM-310 centrifugal mixer was used at 2000 RPM for 30 seconds to create a homogenous mixture with 30% weight ZnS:Cu and 70% weight PDMS. A small amount of the mixture was then cast on a glass slide and placed in a SETCAS KW-4B spin coater. The sample was spun at 200 RPM for 20 seconds and then 2000 RPM for 30 seconds producing a sample of 0.06mm thickness. After the spin coated sample was cured, a second layer of 100% PDMS and 0.5mm thick was cast on top to reinforce the film and allowed to cure. After curing, the sample was subjected to high strains above 50% before being allowed to relax. The sample was then mounted on a linear stretcher and placed on a Nikon Eclipse Ti2 optical microscope. The linear stretcher was used to induce uniaxial strain on the sample and hold under tension when making observations of the matrix and particle interactions.

2.3 Data capture

To capture information on the light emission from samples, a TA Instruments Electroforce 3300 tester controlled with WinTest software was used to stretch samples to a particular waveform profile. Information of the gripper displacement and force was recorded.

In order to capture light emission without interference from ambient lighting, a container was constructed around the testing rig to block ambient light, a schematic can be seen in Figure 1.

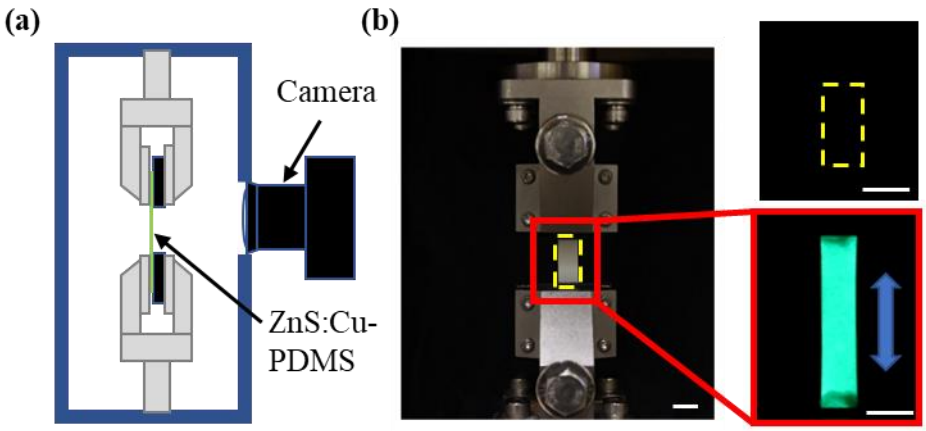

Figure 1: (a) ZnS:Cu-PDMS Tensile sample setup schematic of sample with enclosure **(b)** Sample in Electroforce tester grippers under room lighting. Detail images of sample before stretching and emitting light during stretching in enclosure. Scale bar is 10mm.

The light from the sample was captured in video form by a Canon EOS 90D with a EF24mm f/1.4L II USM lens at 59.9401 fps. The video stored image data for each pixel at a bit depth of 8 bits for each color channel: red, green, and blue.

2.4 MATLAB Processing and Normalization

Using the Visual Processing toolbox in MATLAB, a cropped region of interest was established. Individual frames were then analyzed using MATLAB version R2022a software to convert RGB light values to grayscale using a weighted sum:

$$\text{Grayscale value} = 0.2989 * R + 0.5870 * G + 0.1140 * B \quad (25)$$

Where each value R, G, B is related to the color channel red, green, and blue respectively. This grayscale value was averaged for the entire cropped region of interest to produce a light intensity value, an example of the cropping and conversion to grayscale can be seen in Figure 2.

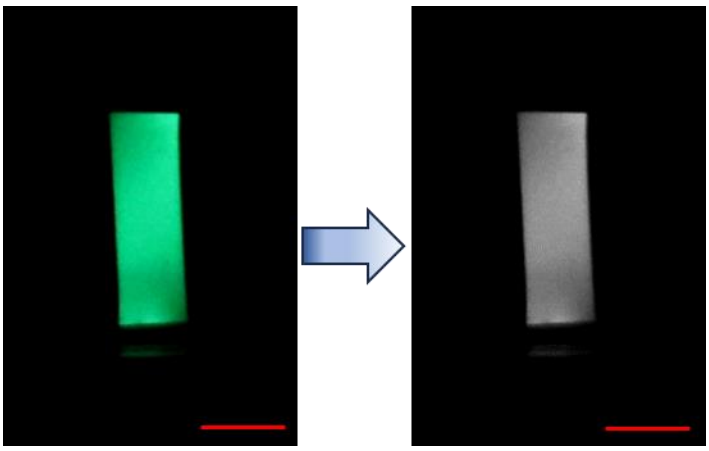

Figure 2: Example frame of area of interest. Resultant analyzed image in grayscale. Scale bar in red is 10mm.

Unless otherwise noted, the cropped region of interest was selected to include the entire sample at maximum stretch and was held to a consistent size for a comparative set of samples.

In order to adjust for variation in sample thickness, a normalization factor is applied to the light intensity values. The grayscale light intensity value is normalized by the relative thickness of samples in a set used for comparison. It is then normalized by the greatest intensity value in a set of samples for a relative comparison.

$$I_{Avg} = \frac{\sum Pixel\ Values}{\#\ Pixels} * \frac{L_{Max}}{L_{Sample}}$$

$$I_{Norm} = \frac{I_{Avg}}{I_{Max}}$$

Chapter 2 contains material which is being prepared for publication. Yun, Joshua; Li, Chenghai; Cai, Shengqiang. The thesis author was the primary researcher and co-author of this publication.

CHAPTER 3: METHOD OF ILLUMINATION

3.1 Method of Illumination

There are two primary theories for the illumination of ZnS:Cu-PDMS composite under loading. The first theory is based on a coupled mechanism of piezoelectrically induced charge combined with electron excitation to produce photons. This method is driven by induced deformations of the particles from stress applied on the particles either by surrounding particles or the PDMS matrix when the sample is subject to stretching. The induced deformation causes a charge that ultimately leads to illumination. The second theory is based on the concept of triboelectrically induced charge that causes the electron excitation from their ground state. Triboelectric charge is generated when two materials of differing triboelectric potential contact each other. Notably, PDMS has been shown to have a very negative triboelectric potential (26). Necessary for the charge generation is the separation of the ZnS:Cu particle and the PDMS matrix at the particle-matrix interface. This separation allows for the relative displacement at the interface of the two materials when combined in the composite. An added complication can arise with the triboelectric theory where the charge is primarily due to a sliding frictional mechanism or due to the separation of contact between the two materials. In order to better understand the driving mechanism behind the light emission, a scenario where the friction can be generated with minimal force or force can be applied with minimal friction can be used to compare light emission.

3.2 Experimental Setup

To make a simplified comparison, two different setups were used. The first, as seen in Figure 3a, was used to test the condition where stress is applied with minimal sliding interaction between the materials and the condition where the two materials separate but do not slide. A thin film, 0.15mm thickness, of PDMS on the end of a rigid body enabled contact and force application between the two materials, but prevented a large degree of relative motion between them that could be induced if the film was thicker. Behind the rigid acrylic body, a cylindrical PDMS plug 8mm long and 8mm in diameter was fitted into a 3D printed adapter socket. 4mm of the plug was left exposed beyond the end of the holder.

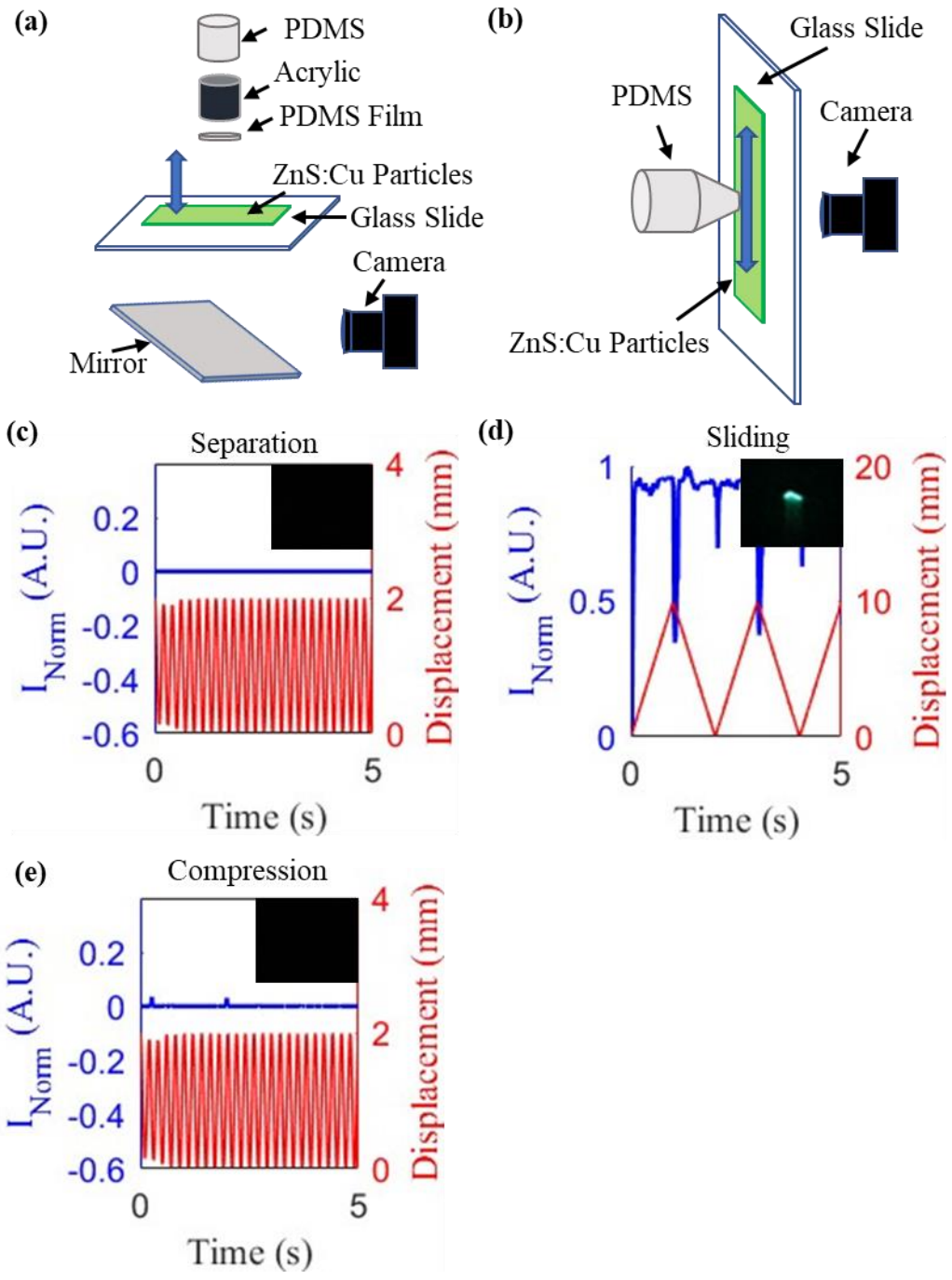

Figure 3: (a) Experimental setup for constant contact compression and alternating contact and interface separation. **(b)** Experimental setup for sliding contact with PDMS in contact with ZnS:Cu particles. **(c)** Normalized pixel intensity of separation contact mode. **(d)** Normalized pixel intensity of sliding contact mode. **(e)** Normalized pixel intensity of compression contact mode.

The plug was used to allow control of the experiment by displacement which resulted in compression force applied on the plug and film. The ZnS:Cu particles were held in place on a glass slide

using transparent double sided scotch tape. One side of the tape was adhered to the glass surface and the other was completely covered in the ZnS:Cu particles. Any excess particles not adhered were removed from the plate before running the experiment. The sample was placed on top of a clear stand with a mirror below to allow direct viewing of the underside of the interface with the camera. Both the compression and separation tests were performed with a compressive sine wave displacement of 2mm and a frequency of 5 Hz with examples of the displacement in Figure 3c-e. The starting point of the film during the compression test was in contact with the particles and the separation tests was offset from the particle surface before starting the test.

To induce a primarily sliding frictional effect, the setup was rearranged as seen in Figure 3b. A tapered plug with a contact circular cross section of 1mm diameter made from 100% PDMS, with the aid of a 3D printed adapter, was placed in contact with the particles mounted on the slide. The tapered plug was then moved across the surface of the ZnS:Cu particles to create frictional interactions. This was done with a triangular waveform with a displacement of 10mm and a frequency of 0.5 Hz. The tapered shape was to help mitigate jamming of the plug against the surface of the particles and provide a more constant contact force. A camera behind the mounting slide and particles was used to record the light emission from the interactions. The interface of the particles and the PDMS remained in contact during the entirety of the test.

3.3 Light Emission Results

The resulting light emission behavior from the different scenarios as seen in Figure 3c-e provides a strong contrast. Unlike other tests, the light intensity value was derived only from the brightest pixel during the entirety of the test. Due to the different sizes of the interfaces this should provide a more reasonable quantity for comparison. Light detected from the compression test was very low and does not appear to follow any kind of pattern that indicated a direct relationship with the loading pattern. There is a similar pattern of behavior from the separation mode experiment, light emission response did not seem to be directly related to the cycles of contact and separation. The light that may have been emitted from

the cyclic separation and contact did not induce a level of detectable light by the camera. In contrast, light from the sliding experimental setup was clearly present; even though the contact area was small, the light from the contact area was relatively bright. When the sample changed directions, there was a momentary pause in velocity and the light quickly decayed but returned to a relatively steady behavior when the sample moves in the other direction.

3.4 Microscope Observations

In order to investigate the physical interactions between the particles and the matrix in the material as it was stretched; a thin sample was investigated with an optical microscope. The sample was mounted to a linear stretcher that was actuated by turning a lead screw. When the sample was stretched to a specified strain, the stretcher was used to hold the sample position and an image was recorded and used for comparison. The Nikon Eclipse Ti2 microscope was used with brightfield light with a polarizing filter. Images were captured with both a 10x magnification and 60x magnification nosepiece. As seen in Figure 4 as the sample was stretched to higher strains, the interfaces of some particles begin to separate. The first separation became visible at around 5% strain, with the size of the pocket growing with each increase in strain.

As strain was increased further, more instances of interfacial separation become apparent and the size of the void also increased. The thin film setup is useful for demonstrating a simplified version of the interaction in a planar form. For tensile samples where the particles are spread in a relatively homogenous manner, including through the sample thickness, relative effects between particles will include interactions in all directions. Depending on the characteristics of the geometry of the particle, location relative to other particles, and possible presence of defects in the matrix and particle interface, it is likely this debonding will initially happen at different strains (6).

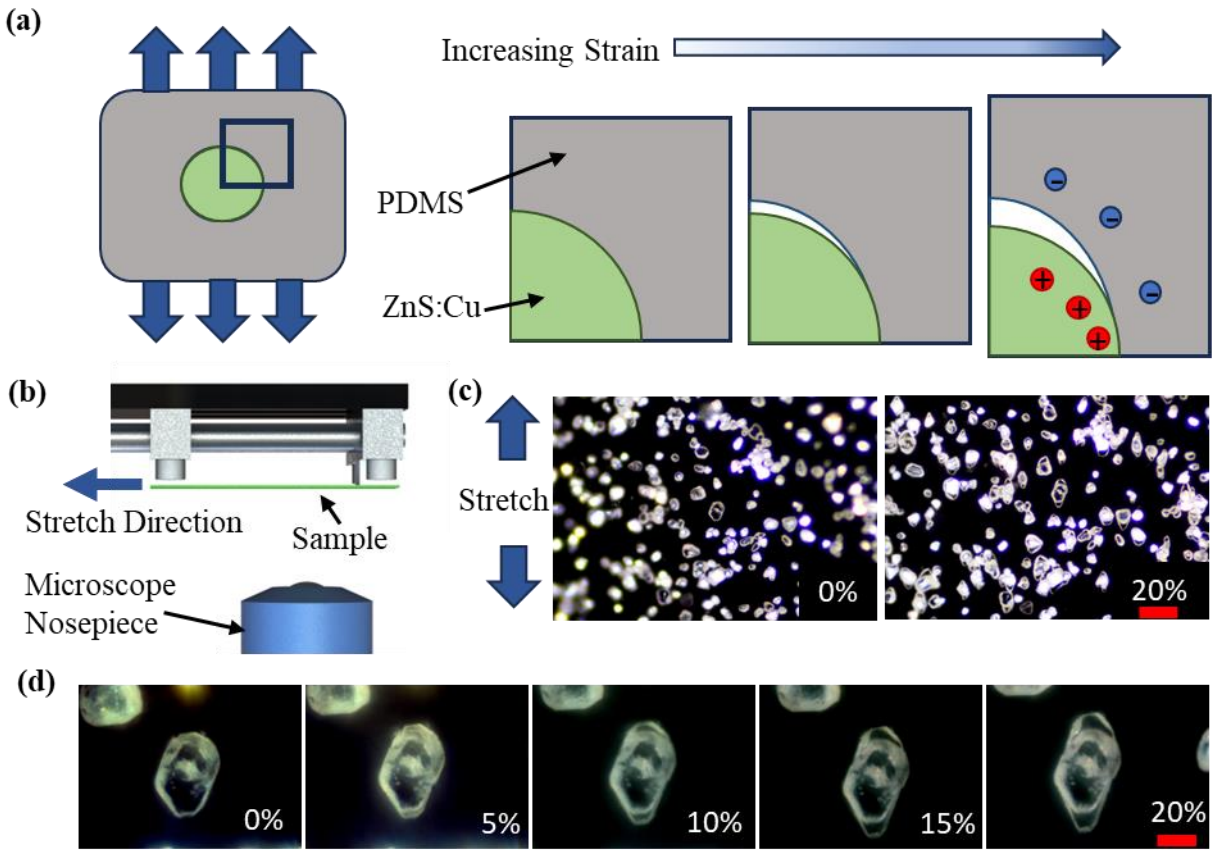

Figure 4: (a) Simplified unit cell schematic of ZnS:Cu-PDMS composite. As strain is increased, the interface separates and subsequent frictional interactions produce triboelectric charge. **(b)** Schematic of stretcher and microscope setup. **(c)** Increasing strain of a previously strained thin film sample. Microscope image of thin film with 10x magnification at 0% and 20% strain from left to right. Scale bar in red is 50 microns. **(d)** Microscope image of thin film with 60x magnification at 0%, 5%, 10%, 15%, 20 % strain from left to right. Start of interfacial separation can be observed at 5% strain. Scale bar in red is 10 microns.

3.5 Discussion

Light emission behavior from the sliding setup had a much higher intensity and also appeared to have a relationship with the applied waveform. This indicated that for the particular combination of materials, the greatest contribution to the observed light is due to the emission induced by a sliding triboelectric phenomenon. It is possible that the additional need for a mirror and transparent layer of acrylic between the particle and PDMS interface and the camera reduced any amount of light perceived during the compression and separation tests. This is unlikely to explain all of the difference between the brightest light detected between the sliding and compression tests. While there would be some loss, the relative intensity is 25 times greater for the sliding case. Additionally, the frequency of waveform is

much greater for the compression and separation cases. If there were significant numbers of photons being emitted, more should be emitted per unit of time in those cases and be indicated as a higher intensity value in the data.

A sliding phenomenon requires the ability of the interface at the particles and matrix to separate and the two materials to have relative displacement. An understanding of the relative stiffness of the materials can provide some intuition to this behavior. ZnS stiffness has been estimated in the order of 10 GPa (27,28) while based on the Shore A hardness of PDMS has Young's modulus is in the order of 1 MPa (29). Based on the Shore A hardness, the modulus can be estimated with the equation:

$$\boldsymbol{log(E_0) = 0.0235S - 0.6403} \textbf{ (29)}$$

Where S is the Shore A hardness and E_0 is the modulus in MPa, which yields 2.6 MPa as an estimate (27). At break the PDMS is expected around 6 MPa. The PDMS is orders of magnitude more compliant than the ZnS material. This difference in modulus between the two materials would tend to create stress concentrations at the interfaces.

As the sample is further subjected to axial strain, the matrix will elongate. Due to the elastomeric nature of the PDMS, the matrix will tend to contract in the lateral direction. This contraction will force contact between the particle surface and matrix in the perpendicular direction to the applied strain as the strain changes. This interaction would occur during both the stretching and relaxation parts of a single axial strain cycle of stretching and relaxation. As the sample is relaxed, the matrix would again slide across the particles as previously opened interfaces return to contact. This sliding motion, with the difference in triboelectric potential, would generate charge that could ultimately excite electrons and cause light emission (6).

Chapter 3 contains material which is being prepared for publication. Yun, Joshua; Li, Chenghai; Cai, Shengqiang. The thesis author was the primary researcher and co-author of this publication.

CHAPTER 4: EFFECTS OF MECHANICAL STIMULI

4.1 Variation of input parameters

Light emission from ZnS:Cu-PDMS composite is related to the total amount of the strain and the strain rate applied to the material. Tensile samples were used in the Electroforce material tester and subjected to triangular cycles of varying maximum strain and strain rate. Tests for investigating strain effects were performed with a strain rate of 100%/s and varying strains of 25%, 50%, 75%, and 100% for 50 cycles. Strain rate effects were tested with a triangular wave at 50% strain and vary rates of 25%/s, 50%/s, 100%/s, and 200%/s. The strain rate samples were first cycled for 50 cycles to reduce any initial transient behavior and data was taken from a single cycle at the prescribed strain and strain rate.

4.2 Strain and Strain Rate Variation

For every cycle of stretching and relaxation, as seen in Figure 5, the sample emitted two major peaks of light that did not correspond to the maximum or minimum strain in a cycle. There was also one smaller peak of light intensity at the maximum strain.

It can also be noted that initially, there was a positive relationship of the strain to the intensity of the emitted light. Samples with a higher maximum strain tended to have a greater emission of light. As the number of cycles progress, the light from the different samples tended to decay. For samples up to 75% strain the decay was relatively even for the different strains, but from Figure 6 it can be seen that at 100% strain there was a sharp decline in light emission within 50 cycles compared to other strains. Figure 6 is derived from the average of 3 samples with the error bars representing the minimum and maximum response from the 3 samples.

The shape of the light response also changed significantly from the 1^{st} to the 50^{th} cycle. The first cycle, shown in black, had a very different peak shape on the stretching portion of the cycle compared to later cycles. For low strain, 25%, the initial stretch emitted very little light. Emitted light was actually higher for the peak on the relaxation portion of the cycle. At higher strains, the shape of the peak showed

an increase in light intensity for most of the stretching cycle. After the initial cycle, the width of the peak narrowed to a distinct increase and decay during the stretching portion of the cycle.

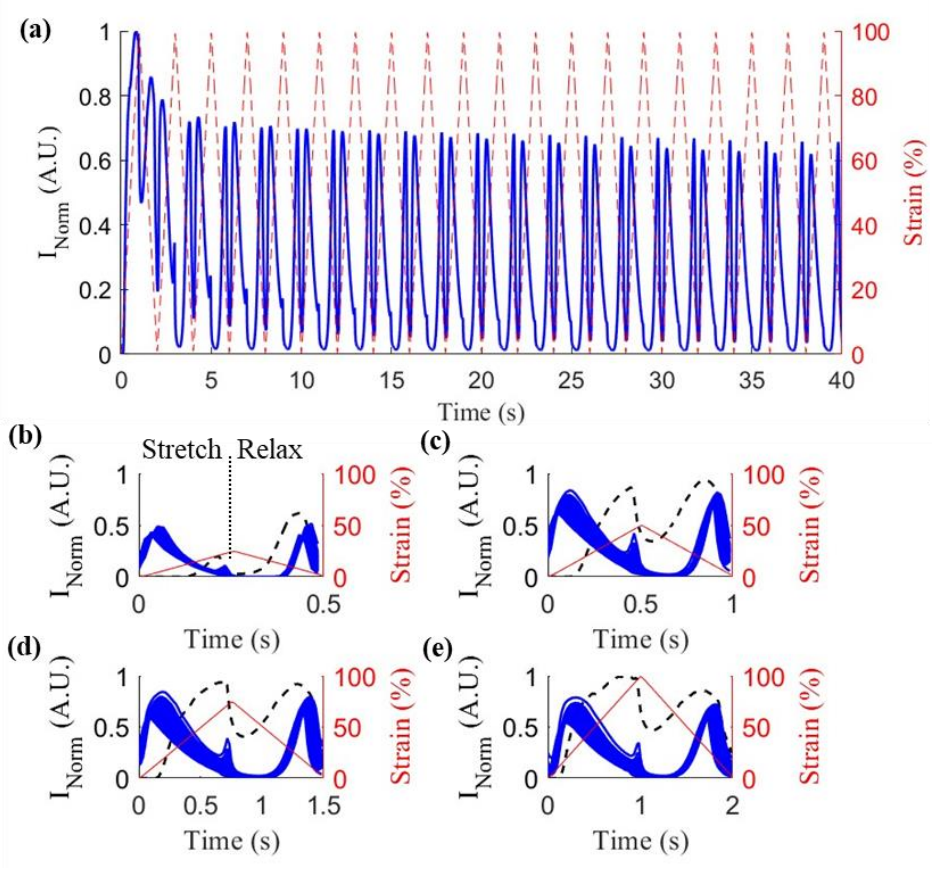

Figure 5: (a) Overlay of light response with cyclic strain application. **(b-e)** Light response vs the time in the stretching cycle 50 cycles at strain levels: **(b)** 25%, **(c)** 50%, **(d)** 75%, **(e)** 100%. Strain rate is kept constant for all trials at 100%/s. Initial cycle show in black, subsequent cycles shown in blue.

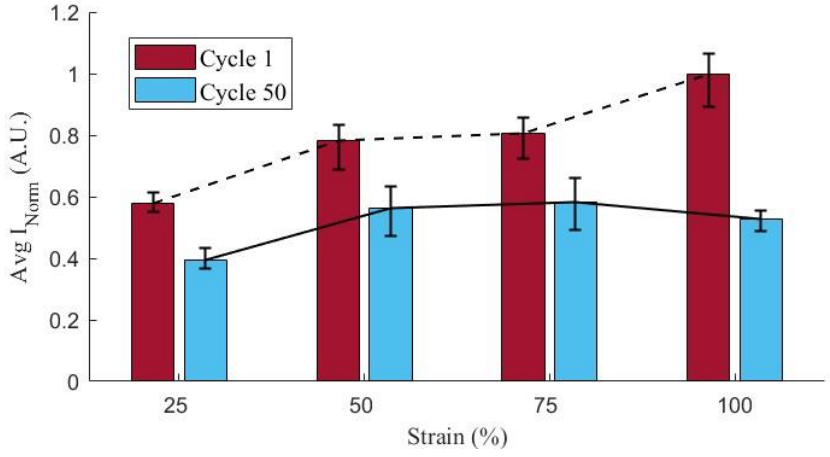

Figure 6: Average maximum light response for the initial and final cycles of a given applied strain

When the strain rate was increased, the emitted light intensity also increased. From Figure 7, is seen that regardless of the strain rate, the pattern of two peaks for a single cycle remained the same. For higher strain rates, 50%/s and above, the relationship between strain rate and emission intensity was relatively linear. At 25%/s the light emission was significantly lower. Results of the average of 3 samples are shown in 7e with the errors bars to indicate the minimum and maximum bounds from the 3 samples.

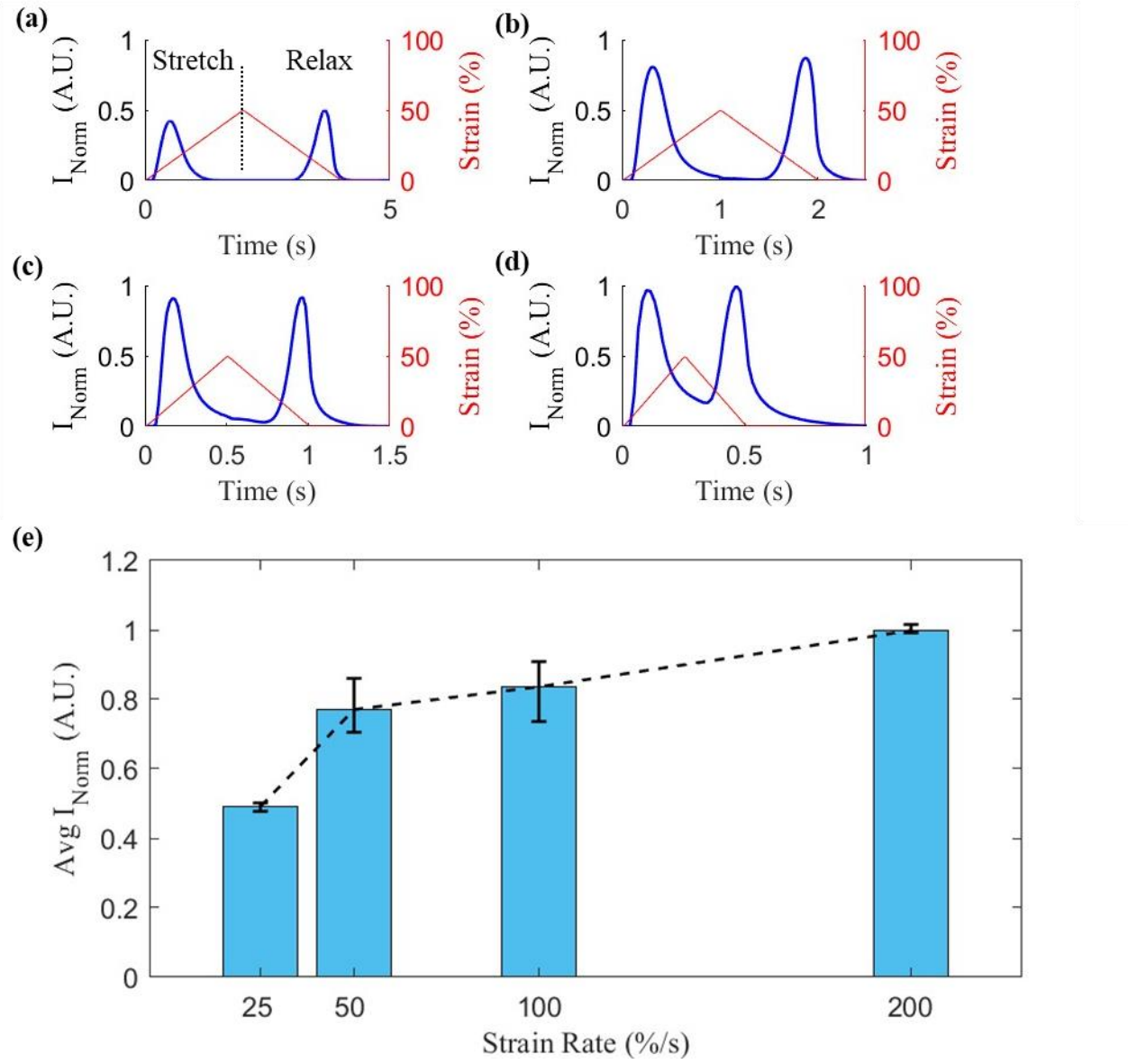

Figure 7: (a-d) Light Response vs the time of a single cycle with varying strain rates: **(a)** 25%/s, **(b)** 50%/s, **(c)** 100%/s, **(d)** 200%/s after stretching for 50 cycles at 50% strain 100%/s. **(e)** Average maximum light response for the cycle at a given strain rate.

4.3 Discussion

It is likely that the overall reduction in luminescence intensity after 50 cycles is due to fatigue of the PDMS matrix. The reduction was most pronounced at the highest strain. This strain level corresponds to the approximate elongation at break for the PDMS matrix. As the polymer is cycled to this limit continuously, it exhibits fatigue and plastic deformation. Since the test was controlled by actuator displacement, this led to a reduction in the actual amount of strain applied to the sample as it elongates due to plastic deformation. This fatigue could also be experienced by the other samples to a less pronounced degree. It is also possible that the samples initially had additional excitation from ambient light or surface charge before they were placed in the testing enclosure, this would lead to a higher initial light emission that would fade with continued cycles.

Another possible contributor for the significantly higher first cycle corresponds to the physical changes that takes place at the particle-matrix interface. For a pristine sample, which has never been stretched, separation of the interfaces would first see a buildup of strain energy before reaching a strain at which the interface would separate. The separation would cause a quick release of strain energy as the matrix springs back from the particle, forcing any interaction between the particle and matrix to occur at a faster rate than later cycles where separation has already occurred and lower strain is needed to separate the interfaces.

The separated interfaces between the particles and matrix act as sites of illumination, the likely reason for the dramatic difference in shape of the first stretching peak compared to subsequent ones is the release of an increasing number of interfaces as strain increases. A higher number of luminescent sites per volume of material would, on a macroscopic level, be perceived as an increase in emission intensity. As the strain increases, more sites begin to separate and luminesce leading to a higher intensity. After the initial bond between the particle and matrix was broken, subsequent bonding is much weaker and has a much smaller range of critical strains that are needed to release the interface and induce frictional interaction. With continued cycles, the number of locations available for luminescence stabilizes and leads to a more repeatable value and pattern of emission.

Presence of a small peak at the maximum strain is also attributed to the opening of new interfaces. With each cycle, and especially at earlier cycles, the stress distribution within the composite changes. Interfaces are no longer firmly attached to particles transfer the axial load in a different manner than the previous configuration. Once particles in one area begin to separate on one cycle, the applied stress on a given area may increase or decrease. At the maximum strain, some interfaces that had a low stress on previous cycles may have a higher stress that causes separation and luminescence.

Chapter 4 contains material which is being prepared for publication. Yun, Joshua; Li, Chenghai; Cai, Shengqiang. The thesis author was the primary researcher and co-author of this publication.

CHAPTER 5 EFFECTS OF CONSTITUENT MATERIAL PARAMETERS

5.1 Sample Parameter Variation

In addition to the mechanical loading on the sample, parameters of the particles and matrix were tested for their effect on the light emission. The ZnS:Cu particles were taken from the powder supplied and sifted to separate particles into different sizes. Tensile samples were then manufactured with these sifted particles and tested for a single triangular waveform cycle at 100%/s strain rate. A different set of samples was also manufactured and was subjected to sets of 5 sine wave cycles at progressively higher strains. Effects of crosslinking in the PDMS matrix were examined by varying the ratios of the two parts of the silicone precursors. Tensile samples for the comparison of crosslinking effects were manufactured with differing ratios and using the particles as supplied without further treatment or purification. These samples were subjected to the same loading patterns as the separated particle size samples, one set for a single cycle and one for progressively greater cycles.

5.2 Experimental Setup and Preparation of Samples

In order to induce particle size variation, the as supplied ZnS:Cu powder was sifted through a series of sieves made with commercial nylon mesh and PVC tubing. The resultant separated powders were then used to create samples with 50% weight ZnS:Cu of a particular particle size range and 50% PDMS.

Samples for crosslinking were prepared in the same manner as a standard tensile sample with the exception of varying the ratio of part A and part B of the precursor. Where part A contains the catalyst and part B contains the crosslinker. The samples were cast with 50% weight ZnS:Cu and 50% of the specified ratio of PDMS.

Three samples of each type either particle size range or mix ratio were tested in the Electroforce and videos recorded of the light emission response to a prescribed strain, strain rate, and waveform.

5.3 Experimental Results of Particle Size Variation

The light emission response from fresh, sifted particle samples for a single cycle is shown in Figure 8, with an example of the applied strain in Figure 8c. Average values of three trials were taken and plotted, with the minimum and maximum values from each set displayed as a shaded area with the dataset. Generally, at larger particle sizes the light was detected at lower strains. For 37-50μm and 50-75μm the light was detectable under 10% strain, while light from smaller sizes was detected later with the smallest around 17% strain. As the cycle continued and strain increased, the light emitted from the 50-75μm samples fell below the 25-37μm samples and was very close to the as supplied particle samples and 10-25μm particles. The 37-50μm particle samples emitted the highest intensity light for the strain measured. Each sample had a generalized shape with a sharper increase in light emission after it was initially detected and a slower increase in light at higher strains.

Even though the light response differed, the overall measured stress as a result of the prescribed displacement from the samples was similar in magnitude. Summarized in Figure 8b, the resulting axial tensile stress is comparable for all samples with a slightly lower value for the 50-75μm samples.

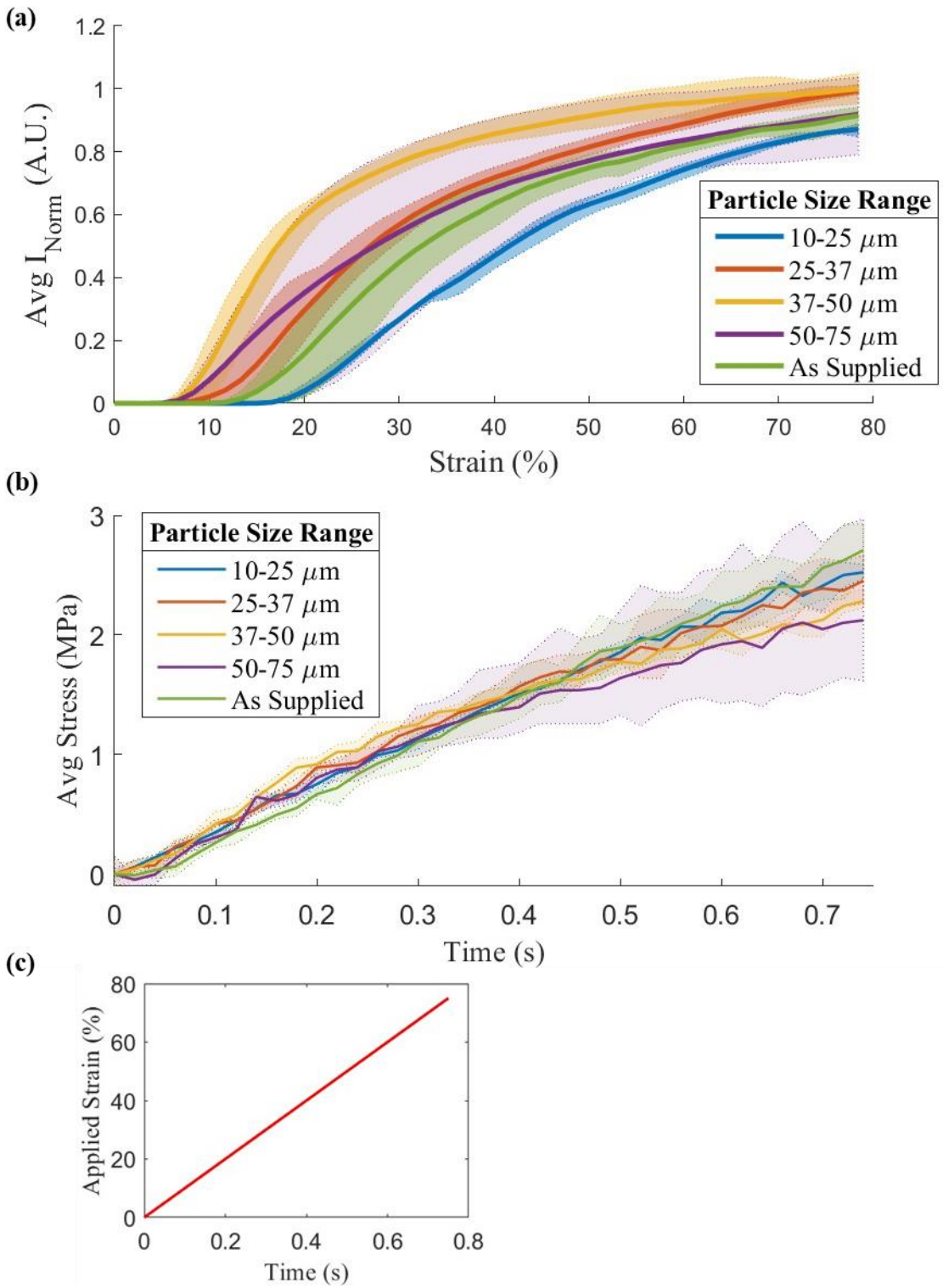

Figure 8: (a) Variation of light emission from a fresh sample with different particle sizes for a single stretching cycle. Filled area represents minimum and maximum bounds from trials. **(b)** Average stress from a single cycle. **(c)** Strain applied to sample to produce light.

When subjected to multiple cycles of a sine wave shape at 0.5Hz in a sweep of increasing maximum strain, the ultimate results show a different pattern. Before data was recorded, the samples were subject to a sine wave displacement of 10 cycles of 20% strain at 0.5Hz. For samples subjected to multiple cycles, the light intensity value was taken as the maximum light experienced during the set of cycles for a given strain level. As seen in Figure 9 the behavior at low strains was similar to the single cycle, with the smaller particle sizes requiring a larger strain to detect light emission. The behavior at higher strains differed in that the smaller particle size samples had a relatively higher intensity at the maximum strain.

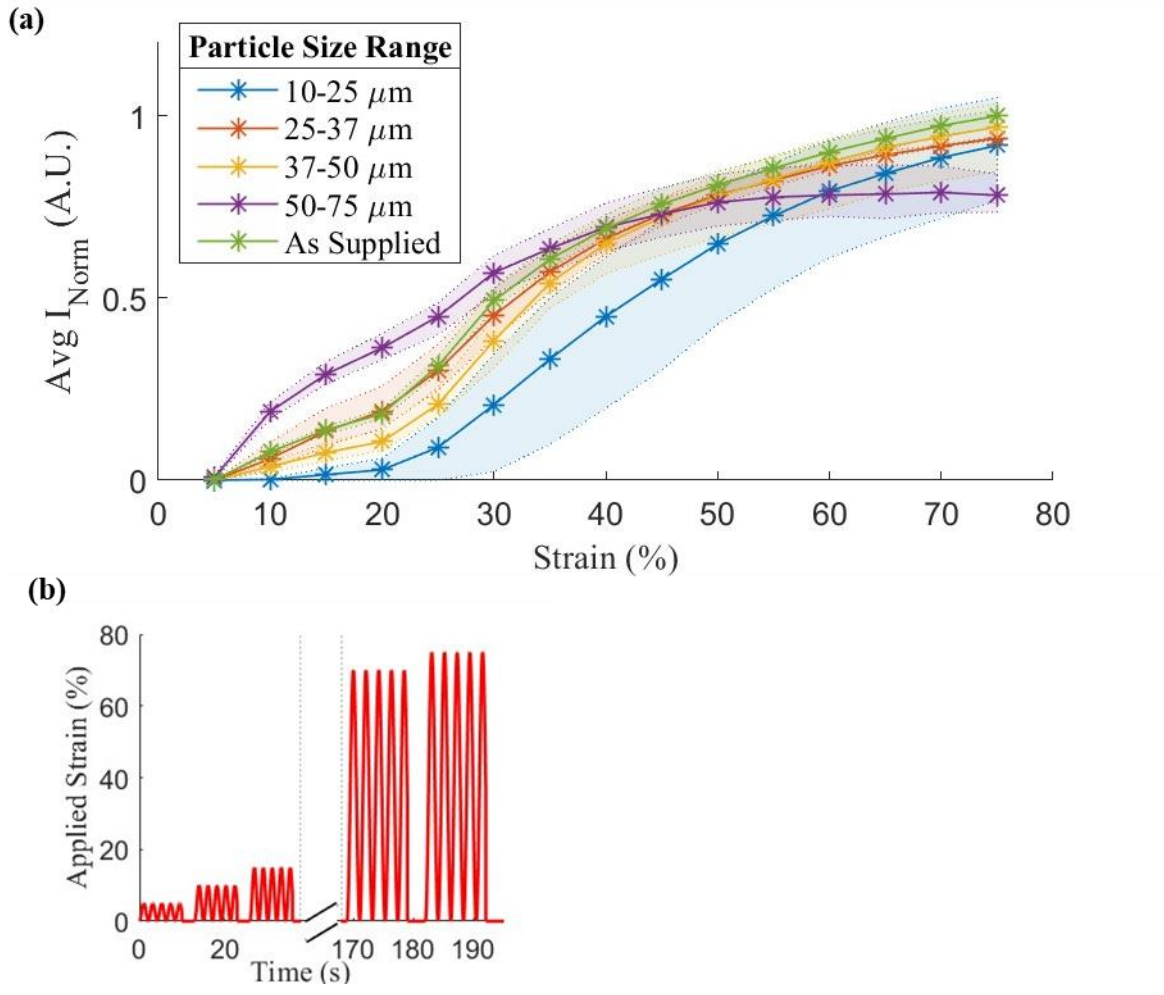

Figure 9: (a) Variation of light emission from sample subjected to multiple cycles with different particle sizes for a single stretching cycle. Light value taken as maximum from cycles from a given strain. Filled area represents minimum and maximum bounds from trials. **(b)** Example of strain applied to sample to produce light.

5.4 Experimental Results of Crosslinking Variation

Emission from varied crosslinking samples for a single cycle, the same as in Figure 8c, is shown in Figure 10. Averages are plotted and the minimum and maximum are displayed as the shaded area. It can be seen there was a dramatic difference in behavior depending on the ratio. For samples that have a very high or low proportion of crosslinker, light was significantly weaker than for samples with a moderate amount. The higher and low ratios were a deviation from the supplier recommended ratio of 9:1. For the 18:1 and 9:1 ratio a relatively strong light emission was observed at low and high strains with a sharp increase in intensity at lower strains near 10% strain and lower increase in intensity at higher strains. Unlike previous samples, the 4.5:1 and 27:1 ratio samples first had detectable light near 30% strain, with a relatively steady increase even at higher strains. The 2.25:1 ratio samples exhibited very dim, almost undetectable levels of light at all strains.

Measurements of average stress in the samples during the cycle showed that a change in ratio did not have a linear relationship with stiffness. The 9:1 sample had the highest stress at 75% strain. Samples with a higher ratio of the part B which contains the crosslinker, 4.5: and 2.25:1 were the next highest stress at 75% strain. The lowest stresses were measured in the samples with the lower ratio of part B, 18:1 and 27:1. This trend was not constant through the entire cycle with the 18:1 ratio samples exhibiting a relatively high stress at lower strains compared to the other ratios.

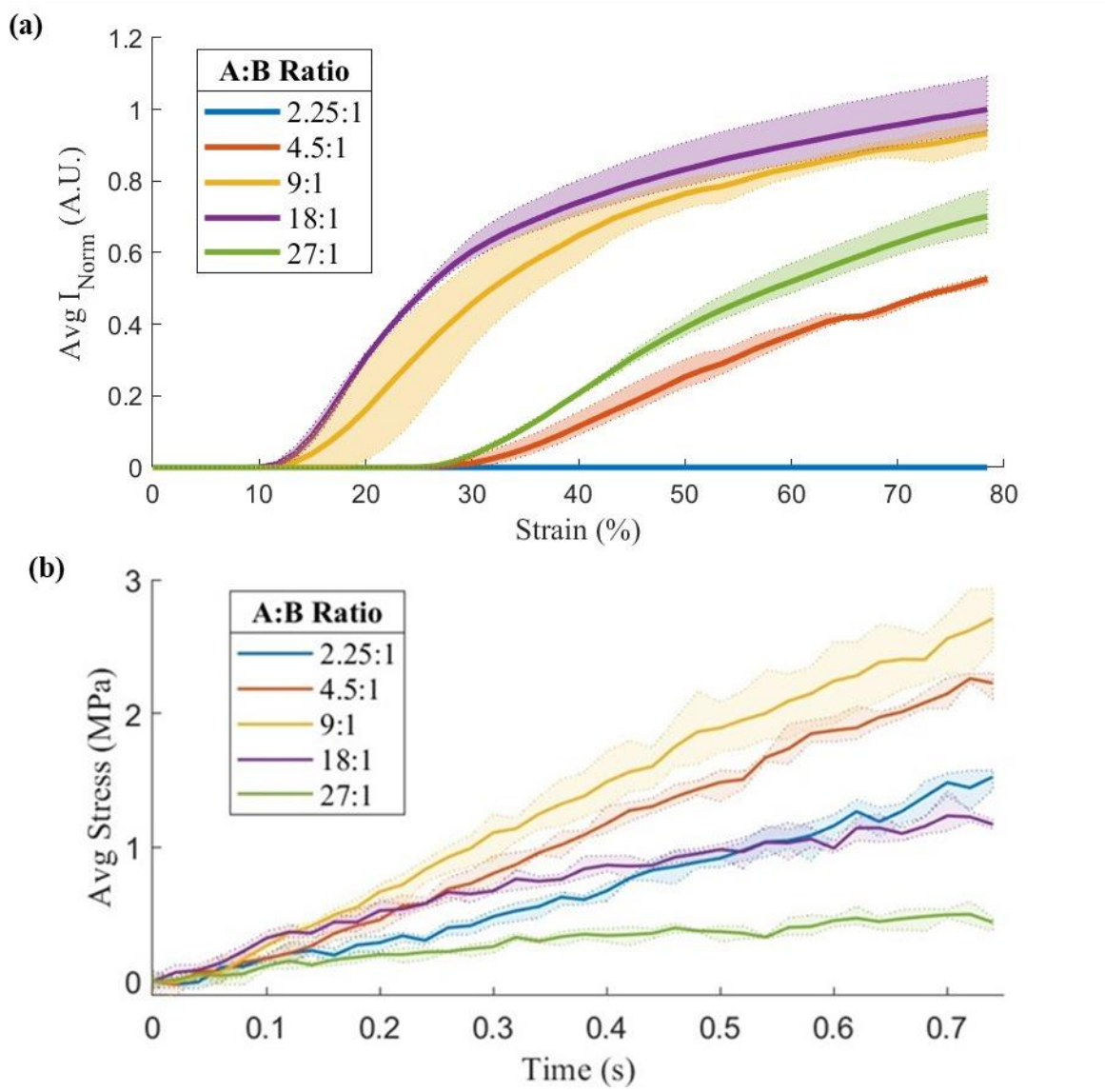

Figure 10: (a) Variation of light emission from a fresh sample with different mix ratios of parts A:B for a single stretching cycle. Part A contains the catalyst, part B contains the crosslinker. Filled area represents minimum and maximum bounds from trials. **(b)** Average stress from a single cycle.

For multiple cycles in a sweep of displacements with increasing maximum strain similar to the one in Figure 9b, the light emission, shown in Figure 11, behavior was similar to the single cycle. Before data was recorded, the samples were subject to a sine wave displacement of 10 cycles of 20% strain at 0.5Hz. Ratios close to the recommended 9:1 ratio and the 18:1 ratio generally had a higher output of light for the same strain compared to samples at more extreme ratios. The samples with a higher and

lower ratio of part A:B than recommended generally had a lower intensity of light emission. Samples with the highest concentration of part B, 4.5:1 and 2.25:1, emitted the lowest amounts of light.

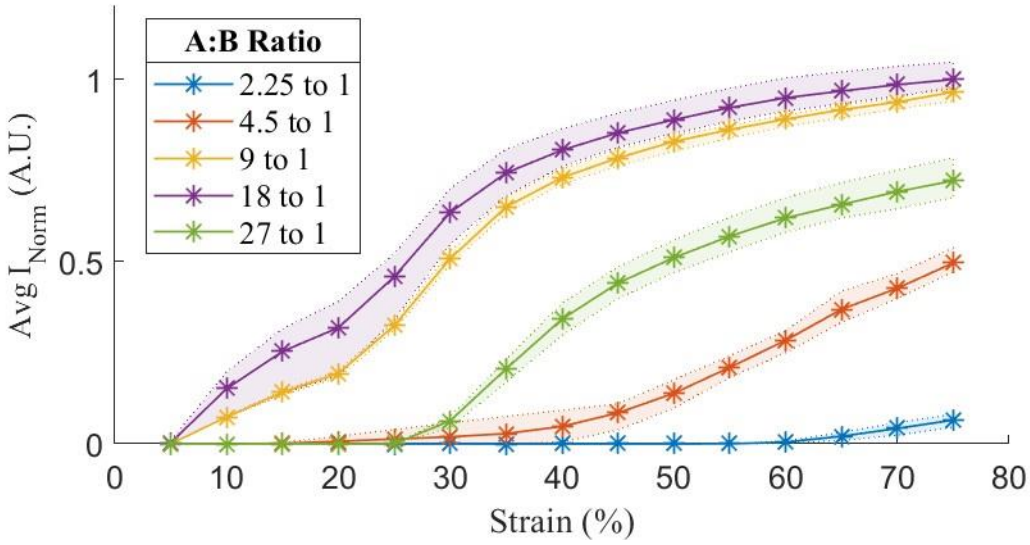

Figure 11: Variation of light emission from sample subjected to multiple cycles at a given strain with different ratios of parts A:B. Light value taken as maximum from cycles from a given strain. Filled area represents minimum and maximum bounds from trials.

5.5 Discussion

The change in light response based on particle size is attributed to the difference in available surface area and stress concentration on the particle matrix interface for different size particles. For samples with the same weight distribution between particles and matrix, a decrease in particle size means an overall increase in particle surface area. Samples with smaller particle sizes will have a greater amount of surface area and more interfaces than those with larger particles. If the same percentage of interfaces were to separates, the total area available for luminescence would be higher. As the strain increases, the increase in light in samples with smaller particles increases at a greater rate than those with larger particles. However, samples with larger particles tend have detectable levels of light emission at lower strains than smaller ones. This is likely due to higher stress concentrations on larger particles than smaller ones (30). A higher stress concentration would increase the likelihood of any given particle-matrix interface of a large particle relative to a small particle. Additionally, the larger surface area of a particle leads to the greater likelihood of a defect, such as a void, existing in the interface. This would also lead to

the separation of the interface at a lower strain than an interface free of defects. The effect of particle size also suggests that other physical characteristics of particle size may yield different results. For instance, processing the particles in such a way to control the overall shape of the particle to more ellipsoid may yield different sensitivities to the same strains.

The variation of response relative to crosslinking density is attributed to the effect of crosslinking on tack and adhesion in the PDMS. The tack of the polymer is considered as the ability of the polymer to wet out surfaces instantaneously while the adhesion is related to the peel strength (31). Samples with relatively low crosslinking density tend to have a higher tack and wet out surfaces quickly (31,32). The PDMS samples with low crosslinking density likely stick to the surfaces of the particles more quickly than the ones with higher crosslinking density. It has been shown for PDMS that as the crosslinking density is increased, the adhesive pull-off force increases (33). This increase in pull-off force could contribute to the lower emission from the highly crosslinked samples as fewer interfaces would separate due to the higher adhesion. Additionally, there may be a contribution to the effect from stress concentrations due to modulus mismatch.

There have been some reports that cover discrepancies in the ratio of crosslinker to stiffness of the PDMS when using high concentrations of the crosslinker (34,35,36). The measured Young's modulus has, in some instances, been shown to decrease and deviate from the relationship between an increasing Shore A hardness and higher Young's modulus with a high concentrations of crosslinker and under tensile load (34,36). With a large increase in crosslinker, the measured Young's modulus can decrease (35). This behavior is attributed to the existence of imperfections due to the off-stoichiometry mix ratio. It is possible the behavior seen in Figure 10b is due to a similar effect, as the ratio of crosslinker is increased the result is a decrease in modulus.

Chapter 5 contains material which is being prepared for publication. Yun, Joshua; Li, Chenghai; Cai, Shengqiang. The thesis author was the primary researcher and co-author of this publication.

CHAPTER 6: STRESS CONCENTRATION

6.1 Stress Concentrations

While light emission in the composite is not necessarily directly caused by applied stress, it does have an effect on the overall intensity. Manipulation of the geometry of the sample creates stress concentrations that tend to lead to areas over higher light intensity.

6.2 Experimental Setup

Here several tensile samples were cast for an exposed sample size of 16x16mm with a thickness of 0.5mm. The PDMS was mixed at the manufacturer specified proportion and combined with the ZnS:Cu particles at a weight percent of 50% to produce the sample. For some of the samples, a hole of a given size was then punched into the sample center to produce areas where stress would be concentrated. Samples were then stretched to 20% strain with a sine wave displacement pattern and a frequency of 0.5Hz to produce light. Light intensity was taken as the individual pixel grayscale value along the estimated centerline of the sample perpendicular to the direction of stretch and then normalized to the highest baseline pixel intensity value.

6.3 Experimental Results

Samples with a hole exhibited a dramatic increase in light intensity from the outer edge of the sample towards the edge of the hole along the centerline. The baseline square sample intensity was relatively constant value from the edge to the center only showing a slight increase. From an overlay of the intensity in Figure 12b,c, it can be noted that the light intensity from the 5mm hole was between 3 and 4 times higher at the maximum value than for the baseline sample and roughly 3 times higher for the 8mm hole sample.

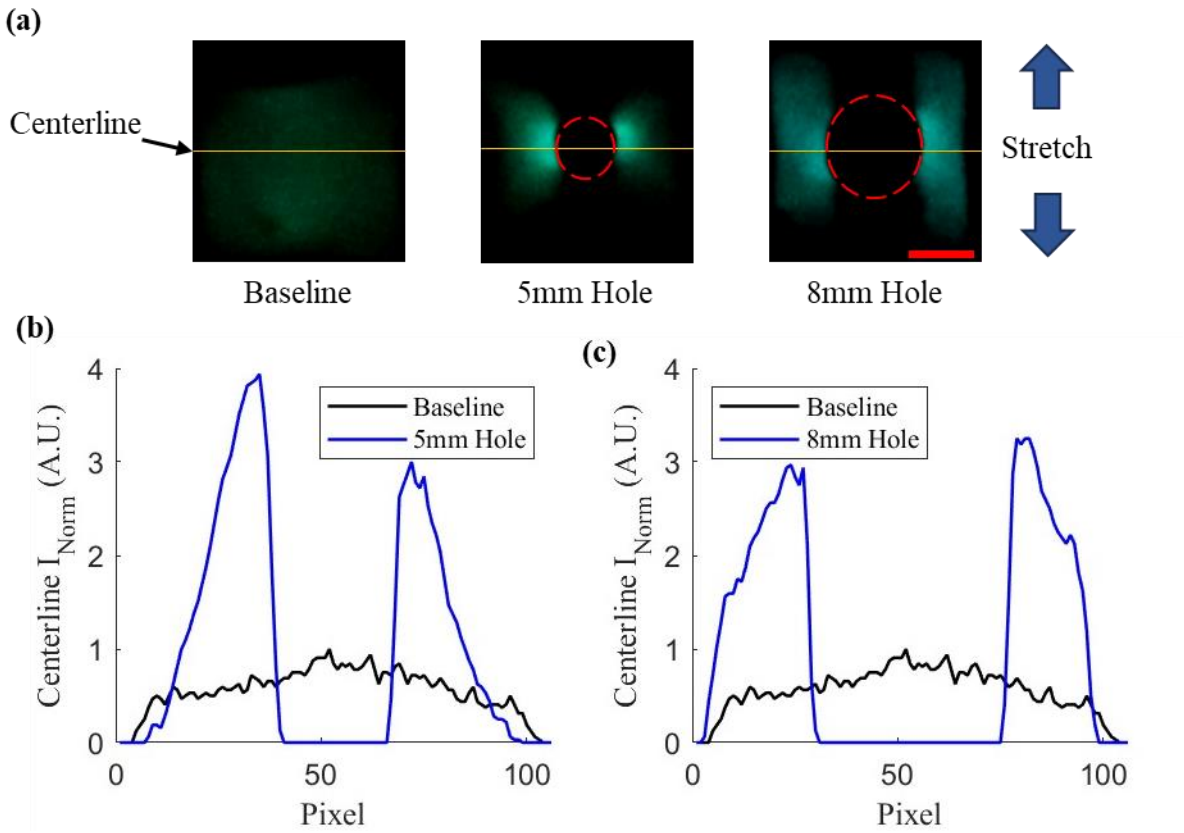

Figure 12: (a) Image of light response for samples under 20% tensile strain cyclic loading. Scale bar (red) is 5mm. **(b)** Overlay of normalized centerline light response for baseline sample and sample with 5mm hole. **(c)** Overlay of normalized centerline light response for baseline sample and sample with 8mm hole.

6.4 Discussion

This increase in light intensity due to the presence of the hole in the sample is associated with the stress concentration. It is well known that the presence of a hole in planar sample will cause stress concentrations in the sides perpendicular to loading when subjected to a tensile load (37,38). With the increase in stress, it is likely that the density of separated interfaces in the region is proportionally higher than in a sample without the stress concentration. With a greater number of locally separated interfaces for a given strain level, an increase in light intensity would be expected. The theoretical maximum value of stress increase for an infinite plate around a hole is 3 times greater than the applied stress (37,38). It is notable the increase in light is close to this proportion and implies that there is some directly proportional relationship between the light intensity and local stress. Since the samples are of a finite size and the stress concentration increase assumes an infinite plate there will be some disagreement between the

behavior especially further from the hole, but the light intensity increase at the hole edge does appear to approximate this expected behavior.

Chapter 6 contains material which is being prepared for publication. Yun, Joshua; Li, Chenghai; Cai, Shengqiang. The thesis author was the primary researcher and co-author of this publication.

CHAPTER 7: HISTORY DEPENDENCE

7.1 History Dependent Behavior

While it is often practice to subject samples to many cycles to observed the light emission, a close examination of the mechanical response with respect to time of a few cycles can also reveal interesting behavior. Light emission behavior from a fresh sample that has never been previously stretched differs significantly from its later behavior under the same strain level. As seen in Figure 5 for a sample that has never been stretched before, on initial stretch the light tends to have an increasing relationship with the applied strain. As the cycle starts to relax, the light intensity fades but eventually has one more spike in intensity before the cycle completes. For stretch and release cycles after the initial cycle a significant change in behavior is observed. The light now has two large spikes, one on the stretch and one on the release portion of the cycle, but now the stretching spike fades much earlier than the initial cycle. In addition, the maximum light intensity decreases from the initial cycle to subsequent ones. After a few cycles the maximum intensity appeared to stabilize at a lower value than the initial cycle.

7.2 Experimental Setup

In order to observed the light and mechanical behavior, an 8x16mm tensile sample with thickness of 0.5mm is cycled in the Electroforce at progressively higher strains of 25%, 50%, and 75% with a triangular waveform with a strain rate of 100%/s for 5 cycles at each strain level. Information about the strain, stress, and emitted light were recorded for comparison. To provide greater fidelity into the change in stress-strain relationship as the sample is cycled, fresh tensile samples were also tested on an Instron 5965 universal testing system under a cyclic tensile load with a 1kN load cell. This loading pattern mimicked the same number of cycles and displacements of the Electroforce tests, but was performed at a lower strain rate of 1%/s instead of the 100%/s of the Electroforce.

7.3 Experimental Results

From Figure 13, it can also be observed that there was also a change in stress-strain behavior in addition to the light intensity. At a given strain level, the stretching portion of the first cycle had a much

higher modulus than the relaxation portion of the cycle which resulted in a large hysteresis loop for the first cycle. Subsequent cycles closely followed a similar stress-strain path to the relaxation portion of the first cycle, they exhibited a much lower hysteresis. When the sample was cycled to a higher strain than it had previously been cycled to, the large hysteresis loop again appeared for the first cycle. After the initial cycle at a given strain level, it was also observed that there was a decrease of maximum stress with each cycle. From Figure 13d, when cycled to 75% strain, the maximum stress decreased with each subsequent cycle though the magnitude of decrease seemed to grow smaller with each cycle.

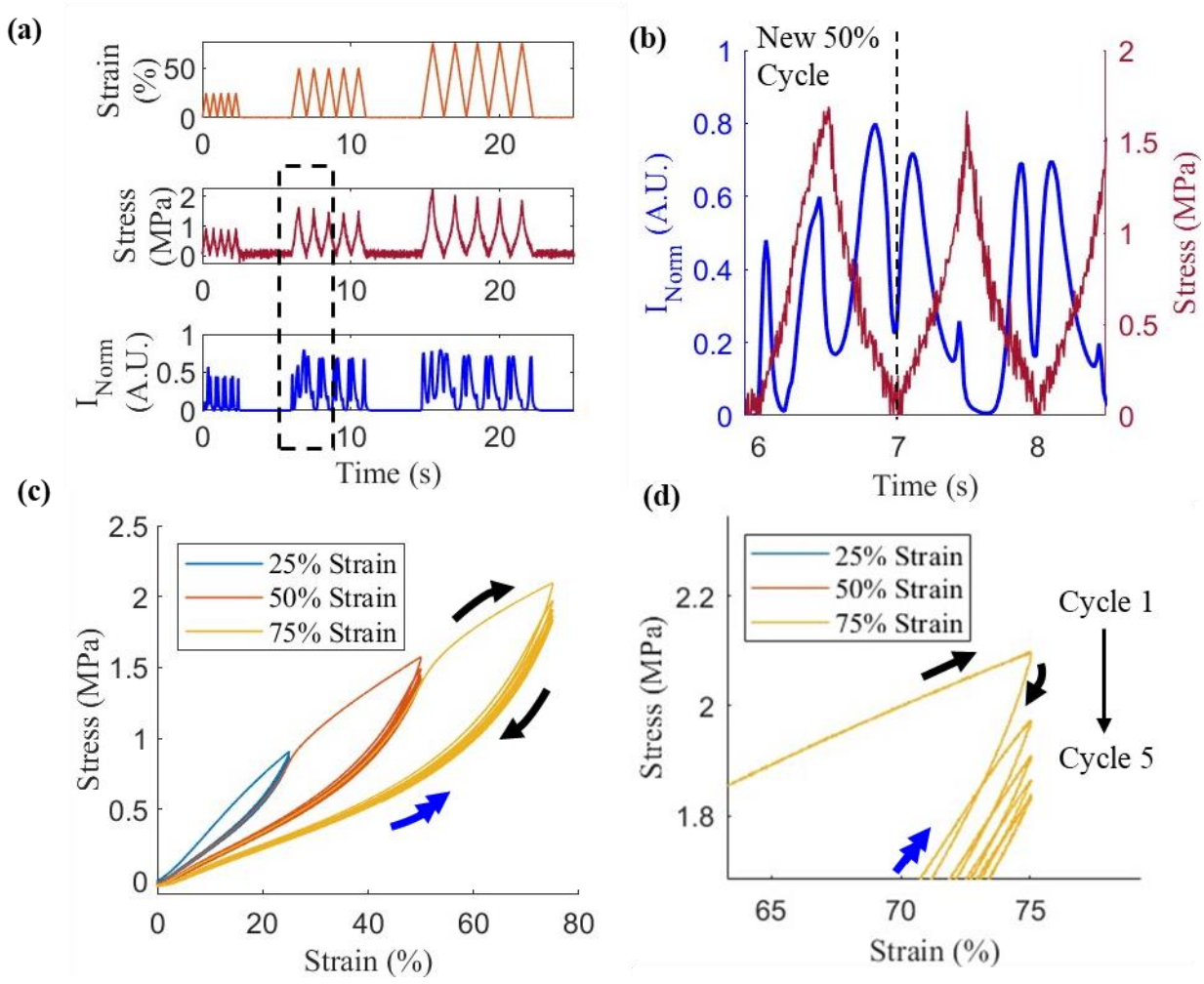

Figure 13: (a) Light response and stress response for sample subjected to 5 triangular waveform cycles at 25%, 50%, and 75% strain with a strain rate of 100%/s. **(b)** Detailed view of light response overlaid with stress for a 50% strain cycle. **(c)** Cyclic stress-strain response of sample from Instron mechanical tester at a strain rate of 1%/s. **(d)** Detailed image of stress response for different cycles at 75% maximum strain.

The first cycle at 50% strain after 25% strain produced light behavior that created 3 peaks for a single cycle of stretch and relaxation. The light and stress response for initial cycle at 50% strain is seen in detail in Figure 13b. On the stretching portion of the cycle, there were two major peaks of light emission with a third during the relaxation of the sample. During the second cycle at 50% strain, it can be seen that this behavior returned to the two major peaks similar to the behavior in Figure 5.

7.4 Discussion

This change in behavior from the initial cycle, both the light and stress-strain, is primarily attributed to the Mullins Effect. The Mullins Effect describes a stress softening effect, most often observed in a filled rubber, that occurs as the result of applied stress (39). There are several physical explanations offered as the mechanism of stress softening, in this composite the mostly likely cause is the observed rupture of the bond at the particle matrix interface (39). As previously stated, it is believed that the separation of the interface between the PDMS and ZnS:Cu particles is a necessary condition to induce illumination in the composite. As the strain increases, more interfaces tend to separate; this leads to more sites that luminesce. Depending on the maximum strain previously experienced by an area of the sample, there will be more or less sites readily available. This debonding also locally alters the path stress takes in the composite as more stress is directly carried by the PDMS matrix. Hysteresis in the material is primarily attributed to the damage to bonds between the particles and the matrix. Previous studies have shown that as a pure material, the PDMS tends to behave in a very elastic manner under cyclic loading (40). There has been some evidence in similar PDMS systems that additional crosslinker also does introduce hysteresis but as the samples were produced at the recommended ratio for these tests it is expected to have a minimal contribution on the first cycle (41).

The debonding also plays a role in creating the three major instances of luminescence in the composite seen in Figure 13b at the first instance of being stretched to a higher strain after being cycled at lower one. Sites that have previously been separated typically require a lower displacement to be separated (6). As a result, first cycling the sample at 25% strain separates a certain number of interfaces.

Then cycling at 50% causes the previously separated interfaces to luminesce creating the first instance at relatively low strains. As the stretching cycle continues, interfaces that previously have remained bonded being to separate and luminesce, creating the second instance of light emission. Finally, the relaxation part of the cycle begins and the interfaces come together, emitting light for the third and final time in the single cycle. With subsequent cycles at 50%, the behavior changes to a much more standard pattern. Each cycle produces 2 major instances of light emission. It can be observed that there was still a relatively small, minor increase in luminescence near the peak strain of a cycle, this is believed to be similar in mechanism but smaller in scale than the previously explained behavior. A small number of interfaces at the peak strain may tend to separate and cause light emission, creating the smaller peak that continues to fade during subsequent cycles.

Chapter 7 contains material which is being prepared for publication. Yun, Joshua; Li, Chenghai; Cai, Shengqiang. The thesis author was the primary researcher and co-author of this publication.

CHAPTER 8: STRAIN DISCRETIZATION RESPONSE

8.1 Strain Discretization

After a number of initial cycles, the number of interfaces that have separated tends to stabilize and the light emission behavior tends to stabilize. As noted by Sauodi each sample is made up of a large number of particles and due to the variations in size, shape, and distance relative to each other the particles have a distribution of critical displacements where the matrix and particle separate (6). The highest intensity of light emission tends to occur when at the greatest concentration of this narrowed distribution. In order to estimate the shape of the distribution, a loading pattern that breaks the loading into discrete steps is used.

8.2 Experimental Setup

An 8x16mm tensile sample with thickness 0.5mm was cycled in the Electroforce at 50% strain with a triangular displacement for 50 cycles at a strain rate of 100%/s and then from 0% strain was subjected to an increase in strain of 5% at a rate of 500%/s and held at the increased strain level for 5 seconds. This 5% increase and hold was then repeated until the 50% strain level was reached. The strain increase causes an emission of light that was recorded while the level hold allows the light to fade before starting the next increase in strain and hold.

8.3 Experimental Results

The overlay of light emission with increasing strain can be seen in Figure 14a. There was an increase in emitted light with the increase in strain that quickly decayed after the level hold began. The largest light emission was roughly centered on the increase from 15%-20% with significant light emission from one level increase at 10%-15% and 25%-30%. The normalized light response for each increase in strain is compared in Figure 14b with the light response overlayed by starting the time at the increase in strain. A summary of the averaged response for three samples can be seen in Figure 14c, averaged values for light illumination at each step were plotted. Error bars were assigned based on the minimum and maximum recorded values from the three trials. At the high and low ends of the range from

0%-50% strain, there was little to no light emission. In the central part of the range, there was a greater instance of emission.

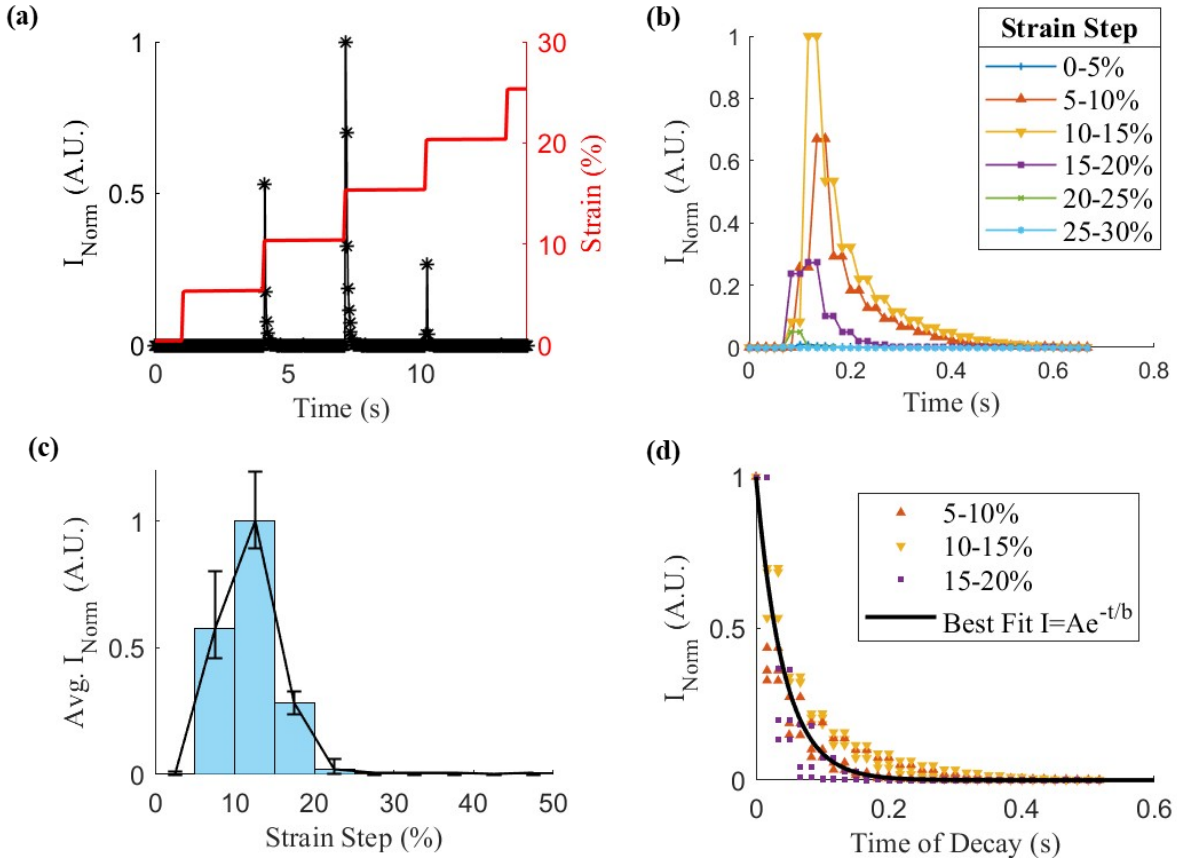

Figure 14: (a) Light response of sample subjected to a progressive, uniaxial stretch and hold loading after initialization cycling. **(b)** Light response after each subsequent increase in strain. **(c)** Averaged light response from different strain levels. **(d)** Best fit curve of light decay of normalized strain step increments from all trials.

For each of the three steps with the highest emission, the decay of the light was plotted to show the time dependent behavior of the light after the increase. The light emission from each of the three highest light emission steps were normalized to the maximum intensity of emission during the decay period. This was repeated for three trials and then the results were used to create a scatterplot as seen in Figure 14d. The decay is assumed to take the form of a natural exponential function:

$$I_{Decay}(t) \propto A * e^{\frac{t}{-b}}$$

Where the light emission, *I* is proportional to a scaling factor, *A*, depending on the maximum light in each step which is normalized to 1, and decays at a rate described by, *b*, the decay time constant and *t* is the

time in seconds since the decay began. Using a line of best fit for the dataset it was determined that the decay time constant, *b*, is 0.041 ± 0.002 seconds with a 95% confidence interval. The best fit line appeared to closely explain the variation of the data with time with an R^2 value of 0.9.

8.4 Discussion

The shape of the light response with each increase of strain in Figure 14c, suggests that the critical displacement for interface separation and initiation of sliding does not have a linear relationship to applied strain. A maximum at the 10%-15% strain step suggests that the majority of separated interfaces that act as emission sites are active in that range. Decreasing levels of light emission after the maximum suggests that the sites are only active in a certain range of strain. After the interface has been separated, frictional interactions only take place for a certain range of strain after which there is no longer significant light emission.

The trend of the observed decay behavior is implied to be largely independent of the applied strain. When accounting for the intensity at the start of decay, the decay for each step follows a similar trend with a sharp initial decrease that gradually tapers off until it falls beneath the detectable threshold of the camera sensor. This decay time estimation is very close to the value previously reported by Saoudi of 0.04 seconds (6). As well, it is close in value to some reports given for photoluminescence in ZnS:Cu:Cl or ZnS:Cu:Al (42) of 0.05 and 0.035 seconds respectively (42). It does differ significantly from the reported values from electroluminescence in the same phosphor of between 4 and 370 microseconds (43). There is the possibility that discrepancies between the results emerge as this test setup does not distinguish between individual wavelengths of light and the decay lifetime has been noted to have frequency dependence or the luminescence coming from a different mechanism of excitation (43).

It is likely that some variability in the data is due to the ability of the sensitivity camera to detect light. The light emitted from the sample at low strain increments tends to be low in intensity. As the light decays, it eventually falls beneath the threshold of the sensor which can truncate some of the decay. This would have an especially significant effect on the decay time of the steps with low initial intensity as the

decay may fall below the threshold before many data points can be taken. As well, the physical setup does introduce limitations on the rate of the change in strain as it cannot instantaneously accelerate or stop.

Chapter 8 contains material which is being prepared for publication. Yun, Joshua; Li, Chenghai; Cai, Shengqiang. The thesis author was the primary researcher and co-author of this publication.

CHAPTER 9: CONCLUSION

The ML of ZnS:Cu-PDMS composite has been of interest to researchers due to its potential for use in a multitude of applications. While the light emission due to mechanical stimuli shows promise in adding functionality without a dedicated supply of electrical power, the underlying relationship between the cause of light emission and stimuli has some gaps in understanding. Among the gaps are the change in light emission behavior as the material is subjected to multiple cycles of loading and changes due to the variation of the constituent materials. In this thesis, a simplified model of interaction was used to explore the interaction that leads to light emission. The light emission and microscope observations suggested that interfacial separation and sliding, frictional interactions, are the primary cause of light emission. Light emission results from the variation of particle sizes and PDMS mix ratios suggested that the light emission response to the strain can vary with significant changes to particle size and complex interactions that result from changes in mix ratio. A relationship between stress softening and the interface separation was attributed to the Mullins effect and the effect on light emission was explored. A proposed distribution between the applied strain and active sites of light emission is explored and decay behavior is characterized. With this improved understanding of the link between the light emission and stimuli, researchers will be empowered to more precisely explore avenues of optimization and application.

REFERENCES

(1) Feng, A.; Smet, P. A Review of Mechanoluminescence in Inorganic Solids: Compounds, Mechanisms, Models and Applications. **2018**, *11* (4), 484–484. https://doi.org/10.3390/ma11040484.

(2) Zhuang, Y.; Xie, R. Mechanoluminescence Rebrightening the Prospects of Stress Sensing: A Review. *Advanced Materials* **2021**, *33* (50), 2005925. https://doi.org/10.1002/adma.202005925.

(3) Monette, Z.; Kasar, A. K.; Menezes, P. L. Advances in Triboluminescence and Mechanoluminescence. *Journal of Materials Science: Materials in Electronics* **2019**, *30* (22), 19675–19690. https://doi.org/10.1007/s10854-019-02369-8.

(4) Jalaal, M.; Schramma, N.; Dode, A.; de Maleprade, H.; Raufaste, C.; Goldstein, R. E. Stress-Induced Dinoflagellate Bioluminescence at the Single Cell Level. *Physical Review Letters* **2020**, *125* (2). https://doi.org/10.1103/physrevlett.125.028102.

(5) Zhang, H.; Wei, Y.; Huang, X.; Huang, W. Recent Development of Elastico-Mechanoluminescent Phosphors. *Journal of Luminescence* **2019**, *207*, 137–148. https://doi.org/10.1016/j.jlumin.2018.10.117.

(6) Saoudi, A. Conversion of Mechanical Energy into Light: Understanding the Phenomenon in the Case of Phosphor-Elastomer Composite Materials. THÈSE de DOCTORAT, Université de Lyon, 2021, pp. 1–155. https://theses.hal.science/tel-03290735/ (accessed 2022-12-16).

(7) Park, Hye-Jeong & Kim, Seongmin & Lee, Jeong Hwan & Kim, Hyoung & Seung, Wanchul & Son, Youngin & Kim, Tae & Khan, Usman & Park, Nae-Man & Kim, Sang-Woo. (2019). Self-Powered Motion-Driven Triboelectric Electroluminescence Textile. ACS Applied Materials & Interfaces. 11. 10.1021/acsami.8b16023.

(8) Qian, X.; Cai, Z.; Su, M.; Li, F.; Fang, W.; Li, Y.; Zhou, X.; Li, Q.; Feng, X.; Li, W.; Hu, X.; Wang, X.; Pan, C.; Song, Y. Printable Skin-Driven Mechanoluminescence Devices via Nanodoped Matrix Modification. *Advanced Materials* **2018**, *30* (25), 1800291. https://doi.org/10.1002/adma.201800291.

(9) Zhao, J.; Song, S.; Mu, X.; Jeong, S. M.; Bae, J. Programming Mechanoluminescent Behaviors of 3D Printed Cellular Structures. *Nano Energy* **2022**, *103*, 107825. https://doi.org/10.1016/j.nanoen.2022.107825.

(10) Wei, X. Y.; Wang, X.; Kuang, S. Y.; Su, L.; Li, H. Y.; Wang, Y.; Pan, C.; Wang, Z. L.; Zhu, G. Dynamic Triboelectrification-Induced Electroluminescence and Its Use in Visualized Sensing. *Advanced Materials* **2016**, *28* (31), 6656–6664. https://doi.org/10.1002/adma.201600604.

(11) Kim, S.; Hsiao, Y.-H.; Chen, Y.; Mao, J.; Chen, Y. FireFly: An Insect-Scale Aerial Robot Powered by Electroluminescent Soft Artificial Muscles. *IEEE Robotics and Automation Letters* **2022**, *7* (3), 6950–6957. https://doi.org/10.1109/lra.2022.3179486.

(12) Kim, Y.; Kim, J.-S.; Kim, G.-W. A Novel Frequency Selectivity Approach Based on Travelling Wave Propagation in Mechanoluminescence Basilar Membrane for Artificial Cochlea. *Scientific Reports* **2018**, *8* (1). https://doi.org/10.1038/s41598-018-30633-0.

(13) Soon Kwan Jeong, Seongkyu Song, Kyung-Il Joo, Youngkyoo Kim, Sung Oh Hwang, Jae Wook Jeong, and Hyunmin Kim. 2014. "Bright, Wind-Driven White Mechanoluminescence from Zinc Sulphide Microparticles Embedded in a Polydimethylsiloxane Elastomer" 7 (10): 3338–46. https://doi.org/10.1039/c4ee01776e.

(14) Wang, N.; Pu, M.; Ma, Z.; Feng, Y.; Guo, Y.; Guo, W.; Zheng, Y.; Zhang, L.; Wang, Z.; Feng, M.; Li, X.; Wang, D. Control of Triboelectricity by Mechanoluminescence in ZnS/Mn-Containing Polymer Films. *Nano Energy* **2021**, *90*, 106646. https://doi.org/10.1016/j.nanoen.2021.106646.

(15) Zhang, J.; Bao, L.; Lou, H.; Deng, J.; Chen, A.; Hu, Y.; Zhang, Z.; Sun, X.; Peng, H. Flexible and Stretchable Mechanoluminescent Fiber and Fabric. **2017**, *5* (32), 8027–8032. https://doi.org/10.1039/c7tc02428b.

(16) Zuo, Y.; Xu, X.; Tao, X.; Xiang Qun Shi; Zhou, X.; Gao, Z.; Sun, X.; Peng, H. A Novel Information Storage and Visual Expression Device Based on Mechanoluminescence. **2019**, *7* (14), 4020–4025. https://doi.org/10.1039/c9tc00641a.

(17) Li, J.; Zhang, Z.; Luo, X.; Zhu, L.; Zhong Lin Wang. Triboelectric Leakage-Field-Induced Electroluminescence Based on ZnS:Cu. **2022**, *14* (3), 4775–4782. https://doi.org/10.1021/acsami.1c23155.

(18) Kang, D.; Pikhitsa, P. V.; Choi, Y. W.; Lee, C.; Shin, S. S.; Piao, L.; Park, B.; Suh, K.-Y.; Kim, T.; Choi, M. Ultrasensitive Mechanical Crack-Based Sensor Inspired by the Spider Sensory System. *Nature* **2014**, *516* (7530), 222–226. https://doi.org/10.1038/nature14002.

(19) Ji, H.; Tang, Y.; Shen, B.; Qian, X.; Cai, Z.; Li, F.; Su, M.; Wu, L.; Ma, Y.; Song, Y. Skin-Driven Ultrasensitive Mechanoluminescence Sensor Inspired by Spider Leg Joint Slits. *ACS Applied Materials & Interfaces* **2021**, *13* (50), 60689–60696. https://doi.org/10.1021/acsami.1c20505.

(20) Ryu, D.; Castano, N. Multivariate Characterization of Light Emission from ZnS:Cu-PDMS Self-Sensing Composites under Cyclic Tensile Strains. *IEEE Sensors Letters* **2018**, *2* (2), 1–4.

(21) Sohn, K.-S.; Timilsina, S.; Singh, S. P.; Choi, T.; Kim, J. S. Mechanically Driven Luminescence in a ZNS:Cu-PDMS Composite. *APL Materials* **2016**, *4* (10).

(22) Chandra, B. P.; Chandra, V. K.; Jha, P. Piezoelectrically-Induced Trap-Depth Reduction Model of Elastico-Mechanoluminescent Materials. *Physica B: Condensed Matter* **2015**, *461*, 38–48. https://doi.org/10.1016/j.physb.2014.12.007.

(23) Chandra, B. P. Luminescence Induced by Moving Dislocations in Crystals. *Radiation Effects and Defects in Solids* **1996**, *138* (1-2), 119–137. https://doi.org/10.1080/10420159608211514.

(24) *ELASTOSIL® RT 601 A/B | Room Temperature Curing Silicone Rubber (RTV-2) | Wacker Chemie AG*. WACKER Website. https://www.wacker.com/h/en-us/silicone-rubber/room-temperature-curing-silicone-rubber-rtv-2/elastosil-rt-601-ab/p/000005741 (accessed 2023-07-08).

(25) *Convert RGB image or colormap to grayscale - MATLAB rgb2gray*. www.mathworks.com. https://www.mathworks.com/help/matlab/ref/rgb2gray.html.

(26) Zou, H.; Zhang, Y.; Guo, L.; Wang, P.; He, X.; Dai, G.; Zheng, H.; Chen, C.; Wang, A. C.; Xu, C.; Wang, Z. L. Quantifying the Triboelectric Series. *Nature Communications* **2019**, *10* (1). https://doi.org/10.1038/s41467-019-09461-x.

(27) Panda, S.; Patnaik, P. Elastic Properties of Zinc Sulfide by Using Generalized Gradient Approximations. *Bulgarian Journal of Physics* **2022**, *49* (3). https://doi.org/10.55318/bgjp.2022.49.3.289.

(28) Alhayek, I.; Gaith, M. The Measurement of Overall Elastic Stiffness and Bulk Modulus in Anisotropic Materials: Semiconductors. *Jordan Journal of Mechanical and Industrial Engineering* **2009**, *4* (1), 55–60. https://doi.org/10.1115/imece2009-10097.

(29) Qi, H. J.; Joyce, K.; Boyce, M. C. Durometer Hardness and the Stress-Strain Behavior of Elastomeric Materials. *Rubber Chemistry and Technology* **2003**, *76* (2), 419–435. https://doi.org/10.5254/1.3547752.

(30) Huang, M.; LI, Z. Size Effects on Stress Concentration Induced by a Prolate Ellipsoidal Particle and Void Nucleation Mechanism. *International Journal of Plasticity* **2005**, *21* (8), 1568–1590. https://doi.org/10.1016/j.ijplas.2004.07.006.

(31) Czech, Z. Synthesis and Cross-Linking of Acrylic PSA Systems. **2007**, *21* (7), 625–635. https://doi.org/10.1163/156856107781192337.

(32) Zosel, A. Effect of Cross-Linking on Tack and Peel Strength of Polymers. *Journal of Adhesion* **1991**, *34* (1-4), 201–209. https://doi.org/10.1080/00218469108026514.

(33) Carrillo, F.; Gupta, S.; Balooch, M.; Marshall, S. J.; Marshall, G. W.; Pruitt, L.; Puttlitz, C. M. Nanoindentation of Polydimethylsiloxane Elastomers: Effect of Crosslinking, Work of Adhesion, and Fluid Environment on Elastic Modulus. *Journal of Materials Research* **2005**, *20* (10), 2820–2830. https://doi.org/10.1557/jmr.2005.0354.

(34) Wilder, E. A.; Guo, S.; Lin-Gibson, S.; Fasolka, M. J.; Stafford, C. M. Measuring the Modulus of Soft Polymer Networks via a Buckling-Based Metrology. *Macromolecules* **2006**, *39* (12), 4138–4143. https://doi.org/10.1021/ma060266b.

(35) Seo, J.-H.; Sakai, K.; Yui, N. Adsorption State of Fibronectin on Poly(Dimethylsiloxane) Surfaces with Varied Stiffness Can Dominate Adhesion Density of Fibroblasts. *Acta Biomaterialia* **2013**, *9* (3), 5493–5501. https://doi.org/10.1016/j.actbio.2012.10.015.

(36) Sales, F. C. P.; Ariati, R. M.; Noronha, V. T.; Ribeiro, J. E. Mechanical Characterization of PDMS with Different Mixing Ratios. *Procedia Structural Integrity* **2022**, *37*, 383–388. https://doi.org/10.1016/j.prostr.2022.01.099.

(37) Meyers, M. A.; Krishan Kumar Chawla. *Mechanical Behavior of Materials*; Cambridge University Press: Cambridge ; New York, 2009; pp. 409–415.

(38) Timoshenko, S.; Goodier, J. N. *Theory of Elasticity, by S. Timoshenko and J. N. Goodier,... 2nd Edition*; McGraw-Hill Book Company, Inc, 1951; pp. 78–81.

(39) Diani, J.; Fayolle, B.; Gilormini, P. A Review on the Mullins Effect. *European Polymer Journal* **2009**, *45* (3), 601–612. https://doi.org/10.1016/j.eurpolymj.2008.11.017.

(40) Jeong, S. H.; Chen, S.; Huo, J.; Gamstedt, E. K.; Liu, J.; Zhang, S.-L.; Zhang, Z.-B.; Hjort, K.; Wu, Z. Mechanically Stretchable and Electrically Insulating Thermal Elastomer Composite by Liquid Alloy Droplet Embedment. *Scientific Reports* **2015**, *5* (1). https://doi.org/10.1038/srep18257.

(41) Kim, T. K.; Kim, J. K.; Jeong, O. C. Measurement of Nonlinear Mechanical Properties of PDMS Elastomer. *Microelectronic Engineering* **2011**, *88* (8), 1982–1985. https://doi.org/10.1016/j.mee.2010.12.108.

(42) Chen, Y. Y.; Duh, J. G.; Chiou, B. S.; Peng, C. G. Luminescent Mechanisms of ZnS:Cu:Cl and ZnS:Cu:Al Phosphors. *Thin Solid Films* **2001**, *392* (1), 50–55. https://doi.org/10.1016/S0040-6090(01)00912-9.

(43) Ibañez, J.; Garcia, E.; Gil, L.; Mollar, M.; Marı´, B. Frequency-Dependent Light Emission and Extinction of Electroluminescent ZnS:Cu Phosphor. *Displays* **2007**, *28* (3), 112–117. https://doi.org/10.1016/j.displa.2007.04.001.